applied sciences

MDPI

Article

Application of a Trajectory Tracking Algorithm for Underactuated Underwater Vehicles Using Quasi-Velocities

Przemyslaw Herman

Institute of Automatic Control and Robotics, Poznan University of Technology, ul. Piotrowo 3a, 60-965 Poznan, Poland; przemyslaw.herman@put.poznan.pl; Tel.: +48-61-224-4500

Abstract: In this work, an application of the trajectory tracking algorithm proposed in the literature for underactuated marine vehicles is presented. The main difference relies on that here the dynamics of the vehicle are expressed in terms of some quasi-velocities (QV). This fact has a double meaning. First of all, it is shown that using the QV, it is possible to control a vehicle in the absence of one variable because the works related to marine vehicles have only concerned fully actuated systems. In addition, a controller using QV provides information that gives some insight into vehicle dynamics and that is not available in classical equations of motion. The simulations done on two 3-DOF models of different underwater vehicles and using two desired trajectories show performance of the considered control strategy. A discussion of the presented control scheme and selected control approaches from recent years was also conducted, and the benefits of the proposed approach were pointed out.

Keywords: underactuated underwater vehicle; nonlinear control; quasi-velocities; simulation

check for updates

Citation: Herman, P. Application of a Trajectory Tracking Algorithm for Underactuated Underwater Vehicles Using Quasi-Velocities. *Appl. Sci.* **2022**, *12*, 3496. https://doi.org/10.3390/app12073496

Academic Editor: Seong-Ik Han

Received: 18 February 2022
Accepted: 26 March 2022
Published: 30 March 2022

1. Introduction

In recent years, autonomous underwater vehicles (AUVs) have been gaining much attention because of their usefulness for various operations. In terms of the availability of input signals, vehicles can be divided into fully actuated and underactuated. Therefore, the control methods in each of these cases are usually different. Furthermore, among many problems, trajectory tracking and path following are of particular interest.

The problem of modeling real underwater or surface vehicles is difficult because the system itself as well as the physical phenomena occurring in it and the environmental disturbances can be taken into account only approximately. In addition, the equations of motion are strongly nonlinear, and many physical phenomena are only partially taken into account. For this reason, there are various methods for modeling dynamics of the system and analyzing its properties. Some of these methods may even allow a more accurate analysis of the vehicle behavior in motion. The issues related to marine vehicle modeling have been considered many times, e.g., in [1–5]. An important issue examined in the literature is the control of underactuated marine vehicles exposed to wind, waves and ocean currents, as shown in [6]. Control in the presence of irregular waves was addressed in [7]. When a marine vehicle may encounter obstacles while performing a control task, it is necessary to solve the collision avoidance problem. This was done, for example, in [8–10]. If the variable ballast has to be taken into account, then it is necessary to modify the equations of motion accordingly as in [11]. Automatic control of a single unmanned surface vehicle pushing a floating payload was analyzed in [12]. Such a problem is difficult to solve because the payload being manipulated is insufficiently controlled and its open-loop dynamics are inherently unstable. Problems related to marine vehicle motion are indicated here by way of example to indicate the various difficulties encountered in building a dynamic model and control strategy.

However, since the purpose of this paper is to try to apply a modified control algorithm to a basic model of a vehicle in horizontal motion, the above problems were omitted in this paper. They are very important at the stage of modeling and construction of the control scheme, but they are not crucial for the topic of this work. Here, the aim is to show that using a velocity transformation for the given vehicle model it is possible not only to track the desired trajectory, but at the same time to have an insight into the vehicle behavior for the model with different parameters and for tracking different trajectories. On the other hand, the mentioned previous problems should be investigated in the future. This paper is limited to the problem of trajectory tracking of a 3-DOF underactuated underwater vehicle moving in the horizontal plane. At present, there are many control methods into this control problem of underactuated AUV. There exist various controllers that have been used for this class of vehicles. If the inertia matrix in the dynamical model is a diagonal one, then the methods representing Lyapunov approach [13–15], sliding mode control (SMC) [16–18], terminal sliding mode control (TSMC) [19,20], the proportional-integral-derivative sliding mode control (PID-SMC) [21], backstepping method [22–24] or backstepping and Lyapunov's methods [25,26], backstepping and SMC [27], backstepping and a composite system method [28], feedback control, backstepping and averaging approach [29], SMC and backstepping based on a neruodynamical model [30,31], and output-feedback represented in [32] are used. Another group of strategies is based on neural networks (NN), e.g., in [33,34]. However, these methods are often a combination of different algorithms, e.g., [35] (NN, SMC), [36,37] (NN, backstepping, SMC) or [38] (an event-triggered adaptive neural fault-tolerant control scheme). Fuzzy logic approach, due to its simple control structure, is also employed to the solution of the trajectory tracking problems as, for example, in [39,40]. One can also find other trajectory tracking methods, e.g., prescribed performance [41,42], model predictive control (MPC) [43], dynamic surface control (DSC) method [44], bounded feedback [45], dynamic inversion method [46], linear algebra approach [47], viability control [48].

Models with a diagonal inertia matrix, on the one hand, indeed simplify the theoretical considerations, but on the other hand, are less of a representation of the actual vehicle. Therefore, algorithms are designed for models with a non-diagonal inertia matrix. Because in this paper an attempt was made to use the quasi-velocities (QV) for a planar vehicle trajectory tracking, therefore we are interested in control algorithms appropriate when dynamics models are described by an inertia matrix containing non-diagonal elements. In relevant control strategies of this type, for example, neural networks [49–52], backstepping method [53,54], sliding mode control [55], input-output linearization [56], an improved line-of-sight (LOS) using terminal sliding mode controller [57], combination of backstepping technique, cascade analysis and Lypunov approach [58], combination of FUO-based observations (finite-time uncertainty observer) and cascade analysis [59], combination of Lyapunov direct method, backstepping control method, and disturbance observer [60] are applied.

The QVs considered in this work are known as the generalized velocity components originally introduced for mechanical systems in [61]. In order to obtain some information, which is inaccessible in classical control algorithms as well as to demonstrate some of the system's properties, quasi-velocities-based controllers were introduced. However, they were also used to fully actuated underwater vehicles control [62,63]. For vehicles with incomplete input signals, the desired trajectory tracking is a big challenge and to the best of the author's knowledge, no effective solution to this problem has been developed. In this work, an attempt was made to describe vehicle dynamics in the sense of the QV and then to apply a known control algorithm. Since this is a preliminary test, methods requiring a combination of different techniques (also including neural networks) have been omitted because they require additional knowledge. Therefore, it was decided to use the input–output linearization method described in [56]. Simulation results show effectiveness of the proposed approach and give a preliminary answer to the question about the applicability of the QV for underactuated underwater vehicles trajectory tracking control.

The originality of the proposed work can be stated as follows:

(i) A proposal for solving the trajectory tracking problem for an underactuated underwater vehicle moving horizontally described by equations resulting from the transformation of the inertia matrix (expressed in terms of the QV);
(ii) Description with the quasi-velocities was used to detect properties of the vehicle model that are not available directly using the classical equations of motion (indication of some information that can be obtained based on the proposed vehicle dynamic equations);
(iii) Controller based on transformed dynamic equations and expressed in QV;
(iv) Simulation verification of the proposed control algorithm for 3-DOF planar models of 2 vehicles with different dynamics and for 2 different trajectories (this issue is important because it happens that the algorithms effectively working in the original literature do not work after changing the parameters of the model or the desired trajectory as demonstrated in [64]). Effects related to the properties of the equations are also presented.

This work is organized in the following way. In Section 2, the problem formulation is presented. In Section 3, equations of motion in terms of the quasi-velocities and the selected tracking control algorithm are described. In Section 4, simulations are given for two different underwater vehicles and two trajectories to demonstrate effectiveness of the modified control scheme. Section 5 contains further discussion concerning the tracking algorithm. Finally, conclusions are made in Section 6.

2. Problem Formulation

The model of the considered marine is presented in Figure 1.

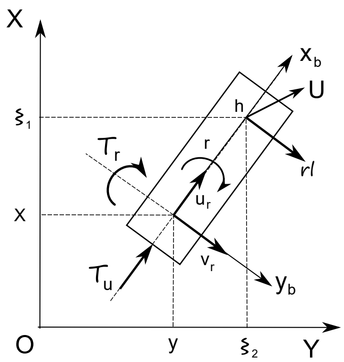

Figure 1. Underwater vehicle model sketch.

The North-East-Down (NED) frame is used. The position and the orientation of the vehicle, in the NED frame, is described by the vector $\eta = [x, y, \psi]^T$. The velocities in the body frame are given by $\nu = [u, v, r]^T$ (the surge velocity, the sway velocity, and the yaw rate, respectively). The vector $V = [V_x, V_y, 0]^T$ represents the ocean current in the NED frame. In the body frame, we have the ocean current $\nu_c = R^T(\psi)V$ ($R(\psi)$ is the rotation between the body frame and the inertial frame). The model of motion of an autonomous surface vehicle (ASV) or an autonomous underwater vehicle (AUV) that moves horizontally is given in the form as in [56,65]:

$$\dot{\eta} = R(\psi)\nu_r + V, \tag{1}$$
$$M\dot{\nu}_r + C(\nu_r)\nu_r + D\nu_r = Bf, \tag{2}$$

where M is the inertia matrix including the added mass, $\nu_r = [u_r, v_r, r]^T = \nu - \nu_c$ represents the vector of relative velocities in the body frame (ν_c is velocity of the ocean current velocity vector). Hence, the Coriolis matrix is denoted as $C(\nu_r)$. Moreover, $f = [T_u, T_r]^T$, where T_u is the thruster force and T_r is the rudder angle (in general applied torque). The matrices $R(\psi), M, C(\nu_r), D, B$ have the form:

$$R(\psi) = \begin{bmatrix} \cos\psi & -\sin\psi & 0 \\ \sin\psi & \cos\psi & 0 \\ 0 & 0 & 1 \end{bmatrix}, \quad M = \begin{bmatrix} m_{11} & 0 & 0 \\ 0 & m_{22} & m_{23} \\ 0 & m_{23} & m_{33} \end{bmatrix},$$
$$C(\nu) = \begin{bmatrix} 0 & 0 & c_{13} \\ 0 & 0 & c_{23} \\ -c_{13} & -c_{23} & 0 \end{bmatrix}, \quad D = \begin{bmatrix} d_{11} & 0 & 0 \\ 0 & d_{22} & d_{23} \\ 0 & d_{32} & d_{33} \end{bmatrix}, \quad B = \begin{bmatrix} b_{11} & 0 \\ 0 & b_{22} \\ 0 & b_{32} \end{bmatrix} \tag{3}$$

where it is assumed that: $m_{11} = m - X_{\dot{u}}$, $m_{22} = m - Y_{\dot{v}}$, $m_{23} = m_{32} = mx_g - Y_{\dot{r}}$, $m_{33} = J_z - N_{\dot{r}}$, $c_{13} = -m_{22}v_r - m_{23}r$, $c_{23} = m_{11}u_r$. The linear damping coefficients matrix D contains the constant elements $d_{11}, d_{22}, d_{23}, d_{32}$, and d_{33} only, whereas B means the actuator configuration matrix.

Referring to [56], the equations replacing Equations (1) and (2) were of the form:

$$\dot{x} = u_r \cos\psi - v_r \sin\psi + V_x, \tag{4}$$
$$\dot{y} = u_r \sin\psi + v_r \cos\psi + V_y, \tag{5}$$
$$\dot{\psi} = r, \tag{6}$$
$$\dot{u}_r = F_{u_r}(v_r) + \tau_u, \tag{7}$$
$$\dot{v}_r = X(u_r)r + Y(u_r)v_r, \tag{8}$$
$$\dot{r} = F_r(u_r, v_r, r) + \tau_r. \tag{9}$$

The quantities were explained in the cited reference.

Next, the change of coordinates vector was defined as $Q = [z_1, z_2, \xi_1, \xi_2, \xi_3, \xi_4]^T$. The new equations of motion had the form: $\dot{z}_1 = z_2$, $\dot{z}_2 = F_{z_2}(z_1, \xi_3, \xi_4) + \tau_r$, $\dot{\xi}_1 = \xi_3 - V_x$, $\dot{\xi}_2 = \xi_4 - V_y$, and also:

$$\begin{bmatrix} \dot{\xi}_3 \\ \dot{\xi}_4 \end{bmatrix} = \begin{bmatrix} F_{\xi_3}(z_1, \xi_3, \xi_4) \\ F_{\xi_4}(z_1, \xi_3, \xi_4) \end{bmatrix} + \begin{bmatrix} \cos z_1 & -l \sin z_1 \\ \sin z_1 & l \cos z_1 \end{bmatrix} \begin{bmatrix} \tau_u \\ \tau_r \end{bmatrix}, \tag{10}$$

where:

$$\begin{bmatrix} F_{\xi_3}(\cdot) \\ F_{\xi_4}(\cdot) \end{bmatrix} = \begin{bmatrix} \cos\psi & -\sin\psi \\ \sin\psi & \cos\psi \end{bmatrix} \begin{bmatrix} F_{u_r}(\cdot) - v_r r - l r^2 \\ u_r r + X(\cdot)r + Y(\cdot)v_r + F_r(\cdot)l \end{bmatrix}, \tag{11}$$

and $F_{z_2}(z_1, \xi_3, \xi_4)$ was obtained from $F_r(u_r, v_r, r)$ by using $u_r = \xi_3 \cos z_1 + \xi_4 \sin z_1$, $v_r = -\xi_3 \sin z_1 + \xi_4 \cos z_1 - z_2 l$, and $r = z_2$. The change of input to linearize the external dynamics was as follows:

$$\begin{bmatrix} \tau_u \\ \tau_r \end{bmatrix} = \begin{bmatrix} \cos\psi & -l \sin\psi \\ \sin\psi & l \cos\psi \end{bmatrix}^{-1} \begin{bmatrix} -F_{\xi_3}(z_1, \xi_3, \xi_4) + \mu_1 \\ -F_{\xi_4}(z_1, \xi_3, \xi_4) + \mu_2 \end{bmatrix}. \tag{12}$$

Theorem 1. *From [56]: Consider an underactuated marine vehicle described by the model (4)–(9). Consider the hand position point $h = [\xi_1, \xi_2]^T = [x + l\cos\psi, y + l\sin\psi]^T$, where $[x, y]^T$ is the position of the pivot point of the ship, l is a positive constant, and ψ is the yaw angle of the vehicle. Then, define $U_d = ((\xi_{3_d} - V_x)^2 + (\xi_{4_d} - V_y)^2)^{1/2} > 0$ as the desired relative velocity magnitude and $\phi_1 = \arctan(\xi_{4_d} - V_y / \xi_{3_d} - V_x)$ as the crab angle.*

The Assumptions (1)–(8) are satisfied.

Assumption 1. *The motion of the vehicle is described using surge, sway, and yaw.*

Assumption 2. *The vehicle is considered as port-starboard symmetric.*

Assumption 3. *The linear hydrodynamic damping is taken into account only.*

Assumption 4. *The constant, irrotational ocean current in the inertial frame* $V = [V_x, V_y]^T$ *is bounded, i.e.,* $\exists V_{max} > 0$ *such that* $(V_x^2 + V_y^2)^{1/2} \leq V_{max}$.

Assumption 5. *The body-fixed coordinate frame b (body frame) is located at a point* $(x_P^*, 0)$*, at a distance* x_P *from the vehicle's center of gravity along the center line of the ship. This point* $(x_P^*, 0)$ *is chosen to be the pivot point, i.e., such that* $M^{-1}B_f = [\tau_u, 0, \tau_r]^T$ *when the model (2) is written with respect to this point. Moreover,* $X(u_r) = -X_1 u_r + X_2$*,* $Y(u_r) = -Y_1 u_r - Y_2$*, and* X_1, X_2, Y_1, Y_2.

Assumption 6. *The following bounds hold on* Y_1, Y_2*:* $Y_1 > 0, Y_2 > 0$.

Assumption 7. *There exist minimum and maximum value constant values* $\underline{\xi}_3$, $\bar{\xi}_3$, $\underline{\xi}_4$, $\bar{\xi}_4$, $\underline{\xi}^*_{3_d}$, $\bar{\xi}^*_{3_d}$, $\underline{\xi}^*_{4_d}$, $\bar{\xi}^*_{4_d}$ *such that:* $\underline{\xi}_3 \leq \xi_{3_d}(t) \leq \bar{\xi}_3$, $\underline{\xi}_4 \leq \xi_{4_d}(t) \leq \bar{\xi}_4$, $\underline{\xi}^*_{3_d} \leq \dot{\xi}_{3_d}(t) \leq \bar{\xi}^*_{3_d}$*, and* $\underline{\xi}^*_{4_d} \leq \dot{\xi}_{4_d}(t) \leq \bar{\xi}^*_{4_d}$.

Assumption 8. *The desired total relative velocity is selected as* $U_d = ((\xi_{3_d} - V_x)^2 + (\xi_{4_d} - V_y)^2)^{1/2} > 0$*. The thrusters of the vehicle provide enough power to overcome the ocean current disturbance.*

Moreover, it is assumed that:

$$
\begin{aligned}
&0 < \bar{U}_d < \frac{Y_2}{Y_1}, \quad k_{v_i} > 0,\ k_{p_i} > 0,\ k_{I_i} > 0,\ k_{v_i}k_{p_i} > k_{I_i},\ i \in \{x, y\},\\
&l > \max\left\{\frac{m_{22}}{m_{23}}, -\frac{X_2}{Y_2}\right\}, \quad \bar{U}^*_d \leq \frac{2\min\{\underline{a}(\underline{d} - \underline{c}), b\}}{\frac{Y_1 \hat{U}_d}{l} + 2\left(Y_1 - \frac{X_1 - 1}{l}\right)}.
\end{aligned} \tag{13}
$$

In controller (12), the new inputs μ_1 and μ_2 are given by:

$$
\mu_1 = -k_{v_x}(\xi_3 - \xi_{3_d}) - k_{p_x}(\xi_1 - \xi_{1_d}) - k_{I_x}(\xi_{1_I} - \xi_{1_{dI}}) + \dot{\xi}_{3_d}, \tag{14}
$$

$$
\mu_2 = -k_{v_y}(\xi_4 - \xi_{4_d}) - k_{p_y}(\xi_2 - \xi_{2_d}) - k_{I_y}(\xi_{2_I} - \xi_{2_{dI}}) + \dot{\xi}_{4_d} \tag{15}
$$

k_{v_x}, k_{v_y}, k_{p_x}, k_{p_y}, k_{I_x}, and k_{I_y} are positive real gains and ξ_I where $i \in \{1, 2, 1_d, 2_d\}$ are integrals of the appropriate signals), guarantees the achievement of the control objectives (i.e., to make the point track the desired trajectory $\Gamma(t) = \{(\xi_{1_d}(t), \xi_{2_d}(t), \xi_{3_d}(t), \xi_{4_d}(t)) | t \in R^+\}$, where $\dot{\xi}_{1_d} = \xi_{3_d}$, $\dot{\xi}_{2_d} = \xi_{4_d}$):

$$
\begin{aligned}
&\lim_{t\to\infty}(\xi_1 - \xi_{1_d}(t)) = 0, && \lim_{t\to\infty}(\xi_2 - \xi_{2_d}(t)) = 0,\\
&\lim_{t\to\infty}(\xi_3 - (\xi_{3_d}(t) - V_x)) = 0, && \lim_{t\to\infty}(\xi_4 - (\xi_{4_d}(t) - V_y)) = 0.
\end{aligned} \tag{16}
$$

Specifically, $(\xi_1, \xi_2, \xi_3, \xi_4) \to (\xi_{1_d}, \xi_{2_d}, \xi_{3_d}, \xi_{4_d})$ globally exponentially and (z_1, z_2) are globally ultimately bounded. Furthermore, the steady-state values of the integral variables give an estimate of the ocean current:

$$
\hat{V}_x = \lim_{t\to\infty} \frac{k_{v_x}(\xi_{1_I}(t) - \xi_{1_{I_d}}(t))}{k_{I_x}}, \quad \hat{V}_y = \lim_{t\to\infty} \frac{k_{y_x}(\xi_{2_I}(t) - \xi_{2_{I_d}}(t))}{k_{I_y}}. \tag{17}
$$

The controller proposed in [56] is called in this work classic (CL).

3. Vehicle Model in Terms of Quasi-Velocities

For a symmetric inertia matrix M, it is possible to use some decomposition method, e.g., [61], which was successfully applied for marine vehicles for example in [62,63] (Equation (1) is valid). In the method $M = \Upsilon^{-T} N \Upsilon^{-1}$, which leads to a diagonal matrix $N = \Upsilon^T M \Upsilon$. Consequently, instead of (2), one gets:

$$\dot{\eta} = R(\psi)\nu_r + V, \quad \nu_r = \Upsilon\zeta, \tag{18}$$
$$\dot{\zeta} + N^{-1}\Upsilon^T C(\nu_r)\nu_r + N^{-1}\Upsilon^T D\nu_r = N^{-1}\Upsilon^T \tau_{ua}, \tag{19}$$

where $\zeta = [\zeta_1, \zeta_2, \zeta_3]^T$, with

$$\Upsilon = \begin{bmatrix} 1 & 0 & 0 \\ 0 & 1 & \Upsilon_{23} \\ 0 & 0 & 1 \end{bmatrix}, \qquad N = \mathrm{diag}\{N_1, N_2, N_3\}. \tag{20}$$

The introduced quantities are defined as: $N_1 = m_{11}$, $N_2 = m_{11}$ $N_3 = m_{33} - (m_{23}^2/m_{22})$, $\Upsilon_{23} = -(m_{23}/m_{22})$, $\zeta_1 = u_r$, $\zeta_2 = v_r - \Upsilon_{23} r$, $\zeta_3 = r$, which means that only $v_r \neq \zeta_2$ because $v_r = \zeta_2 + \Upsilon_{23}\zeta_3$.

Instead of $M^{-1}Bf = [\tau_u, 0, \tau_r]^T$, it is $N^{-1}Bf = [\tau_u, 0, \tau_r]^T$. Equations replacing (1) and (2) are written as follows:

$$\dot{x} = \zeta_1 \cos\psi - (\zeta_2 + \Upsilon_{23}\zeta_3)\sin\psi + V_x, \tag{21}$$
$$\dot{y} = \zeta_1 \sin\psi + (\zeta_2 + \Upsilon_{23}\zeta_3)\cos\psi + V_y, \tag{22}$$
$$\dot{\psi} = \zeta_3, \tag{23}$$
$$\dot{\zeta}_1 = F_1(\zeta) + \tau_u^*, \tag{24}$$
$$\dot{\zeta}_2 = F_2(\zeta) \tag{25}$$
$$\dot{\zeta}_3 = F_3(\zeta) + \tau_r^*, \tag{26}$$

where:

$$F_1(\zeta) = -N_1^{-1}(c_{13}^*\zeta_3 + d_{11}\zeta_1), \tag{27}$$
$$F_2(\zeta) = -N_2^{-1}(c_{23}^*\zeta_3 + d_{22}(\zeta_2 + \Upsilon_{23}\zeta_3) + d_{23}\zeta_3), \tag{28}$$
$$F_3(\zeta) = N_3^{-1}(c_{13}^*\zeta_3 + (c_{23}^* - (d_{32} + \Upsilon_{23}d_{22}))(\zeta_2 + \Upsilon_{23}\zeta_3) - (\Upsilon_{23}(c_{23}^* + d_{23}) + d_{33})\zeta_3), \tag{29}$$

and $c_{13}^* = -(m_{22}(\zeta_2 + \Upsilon_{23}\zeta_3) + m_{23}\zeta_3)$, $c_{23}^* = m_{11}\zeta_1$. The change of coordinates is the same as in [56] because only the velocity transformation was applied and the system dynamics remains unchanged. Therefore, in terms of the QV, one has:

$$z_1 = \psi, \tag{30}$$
$$z_2 = \zeta_3, \tag{31}$$
$$\xi_1 = x + l\cos\psi, \tag{32}$$
$$\xi_2 = y + l\sin\psi, \tag{33}$$
$$\xi_3 = \zeta_1\cos\psi - (\zeta_3 + \Upsilon_{23}\zeta_3)\sin\psi - \zeta_3\, l\sin\psi, \tag{34}$$
$$\xi_4 = \zeta_1\sin\psi + (\zeta_3 + \Upsilon_{23}\zeta_3)\cos\psi + \zeta_3\, l\cos\psi, \tag{35}$$

and also:

$$\dot{z}_1 = z_2, \tag{36}$$
$$\dot{z}_2 = F_3(\zeta) + \tau_r^*, \tag{37}$$

$$\begin{bmatrix} \dot{\xi}_1 \\ \dot{\xi}_2 \end{bmatrix} = \begin{bmatrix} \xi_1 \\ \xi_2 \end{bmatrix} + \begin{bmatrix} V_x \\ V_y \end{bmatrix}, \tag{38}$$
$$\begin{bmatrix} \dot{\xi}_3 \\ \dot{\xi}_4 \end{bmatrix} = \begin{bmatrix} F_{\xi_3}^*(z_1, \xi_3, \xi_4) \\ F_{\xi_4}^*(z_1, \xi_3, \xi_4) \end{bmatrix} + \begin{bmatrix} \cos z_1 & -(l + \Upsilon_{23})\sin z_1 \\ \sin z_1 & (l + \Upsilon_{23})\cos z_1 \end{bmatrix} \begin{bmatrix} \tau_u^* \\ \tau_r^* \end{bmatrix}, \tag{39}$$

where:

$$\begin{bmatrix} F^*_{\xi_3}(\cdot) \\ F^*_{\xi_4}(\cdot) \end{bmatrix} = \begin{bmatrix} \cos\psi & -\sin\psi \\ \sin\psi & \cos\psi \end{bmatrix} \begin{bmatrix} F_1(\zeta) - \zeta_2\zeta_3 - (l + \Upsilon_{23})\zeta_3^2 \\ F_2(\zeta) + \zeta_1\zeta_3 + (l + \Upsilon_{23})F_3(\zeta) \end{bmatrix}. \tag{40}$$

In order to keep the same idea of changing variables as in [56], it was assumed that $u_r = \xi_3 \cos z_1 + \xi_4 \sin z_1$, $v_r = -\xi_3 \sin z_1 + \xi_4 \cos z_1 - z_2 l$, and $r = z_2$. The change of input to linearize the external dynamics has the form:

$$\begin{bmatrix} \tau^*_u \\ \tau^*_r \end{bmatrix} = \begin{bmatrix} \cos\psi & -(l + \Upsilon_{23})\sin\psi \\ \sin\psi & (l + \Upsilon_{23})\cos\psi \end{bmatrix}^{-1} \begin{bmatrix} -F^*_{\xi_3}(z_1, \xi_3, \xi_4) + \mu_1 \\ -F^*_{\xi_4}(z_1, \xi_3, \xi_4) + \mu^*_2 \end{bmatrix}, \tag{41}$$

where μ_1 is defined by (14), whereas μ^*_2 by:

$$\mu^*_2 = -k_{v_y}(l + \Upsilon_{23})(\xi_4 - \xi_{4_d}) - k_{p_y}(\xi_2 - \xi_{2_d}) - k_{I_y}(\xi_{2_I} - \xi_{2_{dI}}) + \dot{\xi}_{4_d}. \tag{42}$$

However, from the used decomposition method, it follows that $\tau^*_u = N_1^{-1}\tau_u$ and $\tau^*_r = N_3^{-1}\tau_r$. This relationship can be used for the input signals normalization, and it is described by the equation:

$$\begin{bmatrix} \tau_u \\ \tau_r \end{bmatrix} = s_f \begin{bmatrix} N_1 & 0 \\ 0 & N_3 \end{bmatrix} \begin{bmatrix} \mu_1 \\ \mu_2 \end{bmatrix}, \tag{43}$$

where s_f means a scaling factor (a constant value). In addition, the following relationships arise from this $\tau_u = s_f N_1 \mu_1 = \beta_1\mu_1$ and $\tau_r = s_f N_3 \mu_2 = \beta_2\mu_2$. It is necessary if the values N_1 and N_3 are too large or too small, which would make the control signal ineffective. The benefit of such normalization is that the control algorithm action will be directly related to the dynamics of the vehicle. Note that in reference [56], the control gains are selected without reference to vehicle dynamics.

Information accessible using QV. Some benefits of decomposition of the inertia matrix can be pointed out:

1. Diagonalization of the inertia matrix instead of computing the inverse inertia matrix;
2. An insight (additional information) into the dynamics of the vehicle;
3. A heuristic algorithm in matching the QV and classical regulator gains;
4. Control signal related to the vehicle's dynamics.

In order to give an insight into the vehicle dynamics, consider some quantities known from the literature that were applied for fully actuated marine vehicles [62,63]. We can use the following of them:

1. Norm of the matrix $\|\Upsilon^{-1}\|$ which determine couplings in the dynamic model of the vehicle. The matrix Υ depend on elements of the symmetric matrix M.
2. The kinetic energy K expressed in terms of the vector ζ for 3-DOF vehicle:

$$K = \frac{1}{2}\nu_r^T M \nu_r = \frac{1}{2}\zeta^T N \zeta = \frac{1}{2}\sum_{i=1}^{3} N_i \zeta_i^2 = \sum_{i=1}^{3} K_i. \tag{44}$$

Because each variable ζ_i takes into account a component of the kinetic energy arising from all other velocities, which are coupled with the i-th variable, then we can examine the contribution of kinetic energy associated with each variable and the total kinetic energy of the vehicle. It is possible to determine K_i reduced by each variable.

3. The average kinetic energy associated with each variable and the total kinetic energy:

$$K_m = \text{mean}\,(K) = \sum_{i=1}^{3} \text{mean}\,(K_i). \tag{45}$$

4. Deformation of each velocity. The variables ζ_i allow one to evaluate the impact of other velocities at the i-th velocity, i.e.,

$$\zeta_i = \Upsilon_{ii}^{-1}\nu_{ri} + \sum_{j=i+1}^{3} \Upsilon_{ij}^{-1}\nu_{rj}. \tag{46}$$

This result means that each ζ_i takes into account a coupling between itself and the other velocities. Thus, using the controller, one can observe the effects of couplings for dynamics of the vehicle. Effect of the dynamical couplings is obtained by Υ_{ij}. As the measure of couplings we introduce the following quantity:

$$\Delta\zeta_i = \zeta_i - \nu_{ri}. \tag{47}$$

For a 3 DOF underactuated vehicle valuable are: (1) the coupling constants and index, (2) kinetic energy distribution into individual variables, (3) errors between the quasi-velocity and the corresponding velocity in the body frame.

4. Simulation Results

Conditions of the investigation done in Matlab/Simulink were as follows: the force and torque values were limited in order to avoid their excessive values at the beginning of the vehicle movement, i.e., $|\tau_u| \leq 5$ N $|\tau_r| \leq 5$ Nm, time of motion $t = 120$ s (for linear trajectory), $t = 300$ s (for sine trajectory), the time step $\Delta t = 0.03$, and using the method ODE3 Bogacki–Shampine. The simulation test was done based on software given in [66].

Two underwater vehicles were intended for the test, namely ROPOS described in [67] and XX AUV model in [53,68]. Their parameters are given in Table 1 and Table 2, respectively. For tracking, the desired trajectory position profiles are assumed, described as $p_d = [x_r, y_r]$:

$$p_d = [0.7\,t,\ 0.7\,t]^T, \tag{48}$$
$$p_d = [0.5\,t,\ 40\sin 0.02\,t]^T \tag{49}$$

linear and sine trajectory, respectively. The start point was $p_0 = [-2,\ \ 6]^T$ (for ROPOS) and $p_0 = [-4,\ \ 8]^T$ (for XX AUV). The starting points were chosen according to the dynamic parameters of the vehicles (due to different dynamics of the tested vehicles), whereas the disturbances $V_x = 0.05$ m/s, $V_y = -0.08$ m/s were taken from [56].

Table 1. Parameters of ROPOS vehicle.

	ROPOS	
Symbol	**Value**	**Unit**
L	1.75	m
W	2.6	m
H	1.45	m
m	2268	kg
J	2457	kg·m^2
$X_{\dot{u}}$	−4380	kg
$Y_{\dot{v}}$	−9518	kg
$N_{\dot{r}}$	−5000	kg·m^2
m_{11}	6648	kg
m_{22}	11,786	kg
m_{23}	−1134	kg·m
m_{33}	7457	kg·m^2
d_{11}	725	kg/s
d_{22}	1240	kg/s
d_{33}	1804	k·m^2/s

Table 2. Parameters XX AUV model.

XX AUV Model		
Symbol	**Value**	**Unit**
L	approx. 1.2	m
m	approx. 45	kg
m_{11}	47.5	kg
m_{22}	94.1	kg
m_{23}	5.2	kg·m
m_{32}	5.2	kg·m
m_{33}	13.6	kg·m^2
d_{11}	13.5	kg/s
d_{22}	50.2	kg/s
d_{23}	41.4	kg·m/s
d_{32}	17.3	kg·m/s
d_{33}	27.2	kg·m^2/s

4.1. ROPOS Vehicle

The parameters of the selected vehicle are given in Table 1 [67]. The ROPOS vehicle has rectangular shape with length L, width W, and height H.

The use of this parameters set means, that $m_{11} = 6648$ kg, $m_{22} = 11{,}786$ kg, $m_{33} = 7459$ kg·m^2 and consequently $N_1 = 6648$ kg, and $N_2 = 11{,}786$ kg, $N_3 = 7348$ kg·m^2. For the point h value $l = 1.3$ m was chosen, where l is the distance between the pivot point in the NED frame described by (x, y) (Figure 1) and the hand position point h.

In [67], the matrix M was a diagonal one. Here, in order to consider the matrix M with off-diagonal elements, it is assumed that $m_{23} = mx_g = -1134$ kg·m, which corresponds to a center of gravity shift of -0.5 m.

For this vehicle $\|\Upsilon^{-1}\| = 1.0493$, which means about 10% couplings (1 is equivalent to 0%, whereas 1.1008 to 20%). This value means that the couplings are weak. Of course, we can take the values of the parameters so that the couplings in the system are larger, but for practical reasons it seems unrealistic.

Linear trajectory. At first, the linear trajectory (48) and using (43) was tested.

The gains for the controller given by (14) and (15) were selected to ensure acceptable errors convergence:

$$k_{v_x} = k_{v_y} = 4, \;\; k_{p_x} = k_{p_y} = 1, \;\; k_{I_x} = k_{I_y} = 0.25. \tag{50}$$

Moreover, due to the dynamics of the ROPOS vehicle $s_f = 10^{-3}$, $s_f N_1 = 6.648$, and $s_f N_3 = 7.348$. Results of simulation are presented in Figure 2. As it is observed from Figure 2a, the actual trajectory reaches the desired trajectory. From Figure 2b,c one can see that all error states $\Delta\xi_i$ tend to zero after about 40 s, which confirms that the algorithm is working properly. The applied force τ_u and torque τ_r (Figure 2d) have big values only if the vehicle starts and then their values are small. In Figure 2e, the kinetic energy corresponding to each variable is given (they are accessible only for the QV controller). The most of the energy is consuming by the ζ_2, which is related to the lateral movement of the vehicle, which means that the lateral velocity v_r plays the crucial role in dissipating this energy. The error $\Delta\zeta_2$ in Figure 2f represents velocity deformation caused by couplings at the beginning of the movement is up to 0.02 m/s is almost an insignificant change.

The kinetic energy average values are $K_m = 4911$ J (and $K_{m1} = 1503$, $K_{m2} = 3401$, $K_{m3} = 7$).

In the next case the gains for the original controller (14) and (15) were assumed the same as in [56] due to a lack of information as to their choice:

$$k_{v_x} = k_{v_y} = 50, \;\; k_{p_x} = k_{p_y} = 5, \;\; k_{I_x} = k_{I_y} = 0.5. \tag{51}$$

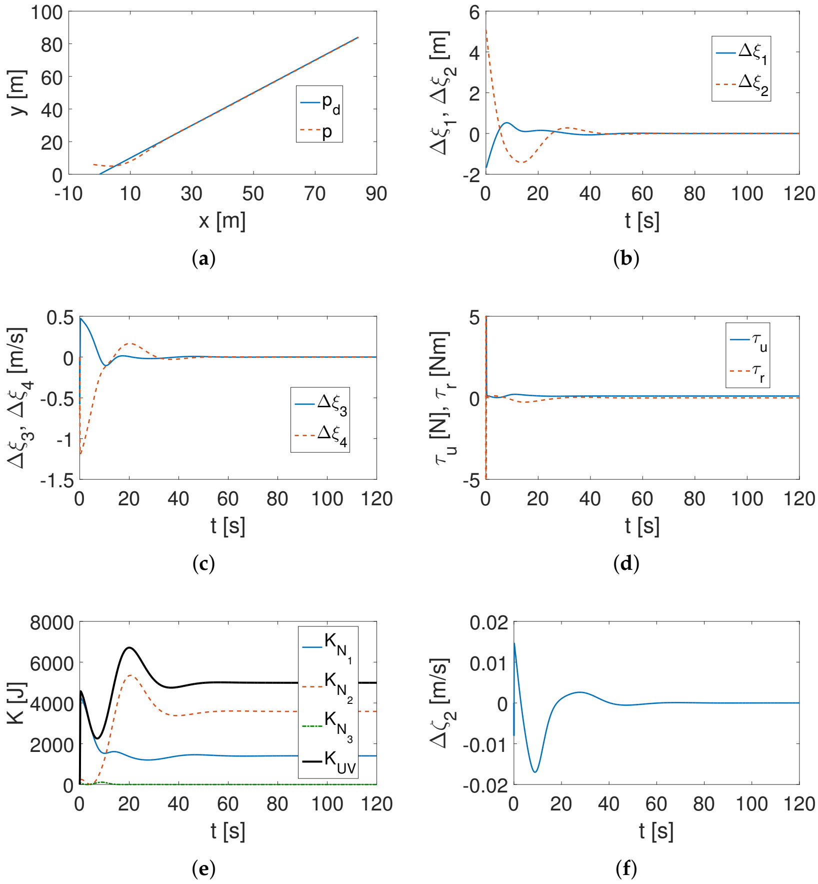

Figure 2. Simulation results for ROPOS QV controller and linear trajectory: (**a**) desired and realized trajectory; (**b**) position error states; (**c**) velocity error states; (**d**) applied force and torque; (**e**) kinetic energy time history; and (**f**) error $\Delta\zeta_2$.

As it follows from Figure 3a the trajectory is reached in a longer time than in the case of the QV tracking algorithm. Additionally, the position errors shown in Figure 3b,c are approaching zero in a longer time (after about 80 s). The applied force and torque have similar values if we compare Figures 3d and 2d. Therefore, it can be concluded that the values of gains have a significant impact on the performance of the control algorithm.

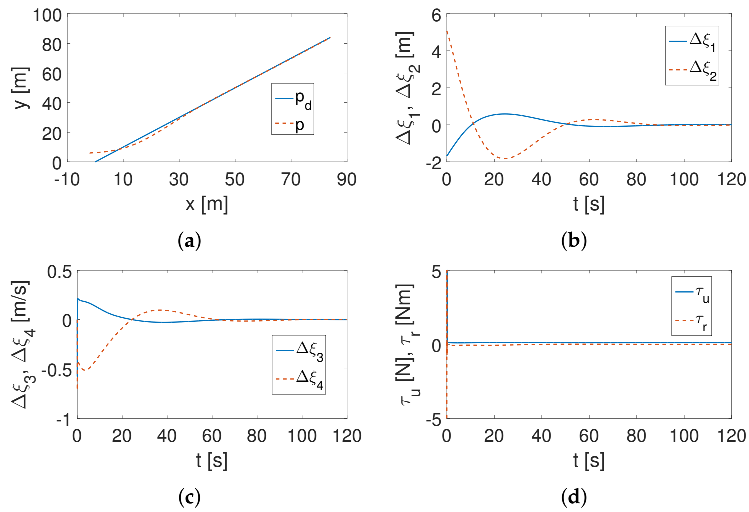

Figure 3. Simulation results for ROPOS original controller (CL) and linear trajectory: (**a**) desired and realized trajectory; (**b**) position error states; (**c**) velocity error states; (**d**) applied force and torque.

Sine trajectory. Next, the sine trajectory described by (49) for ROPOS and using the QV algorithm was investigated. The same gains (50) were used for simulation.

From Figure 4a it is seen that the trajectory is tracked correctly. The state errors are close to zero after about 50 s as it arises from Figure 4b,c. The applied force and torque in Figure 4d have similar values as in Figure 2d. The kinetic energy shown in Figure 4e is consumed mainly by the lateral movement of the vehicle, which also results from dynamic parameters and the error $\Delta\zeta_2$ representing velocity deformation because of the couplings is very small.

The kinetic energy average values are now $K_m = 2418$ J (and $K_{m1} = 702$, $K_{m2} = 1712$, $K_{m3} = 4$).

Figure 5 shows the test results of the original controller (CL). It can be seen that the trajectory is tracked slightly worse despite the small differences visible in Figure 5a. It is because values of the error states (Figure 5b,c) change during the vehicle motion. The controller works worse than the QV controller despite similar applied force and torque values (cf. Figures 5d and 4d).

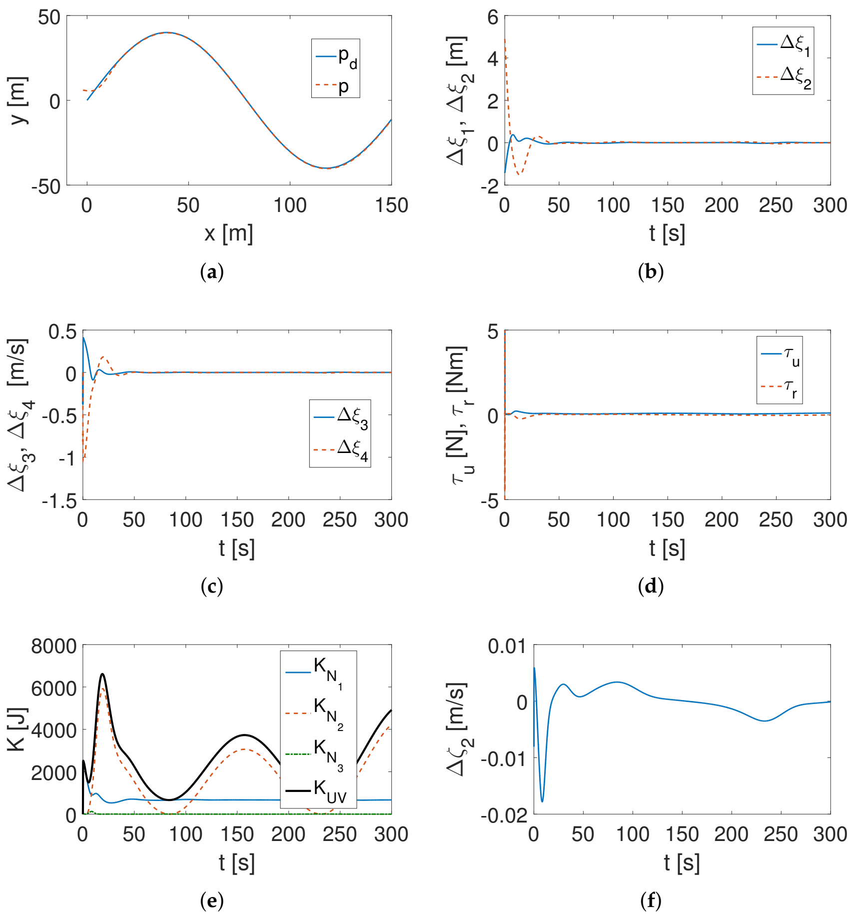

Figure 4. Simulation results for ROPOS QV controller and sine trajectory: (**a**) desired and realized trajectory; (**b**) position error states; (**c**) velocity error states; (**d**) applied force and torque; (**e**) kinetic energy time history; and (**f**) error $\Delta\zeta_2$.

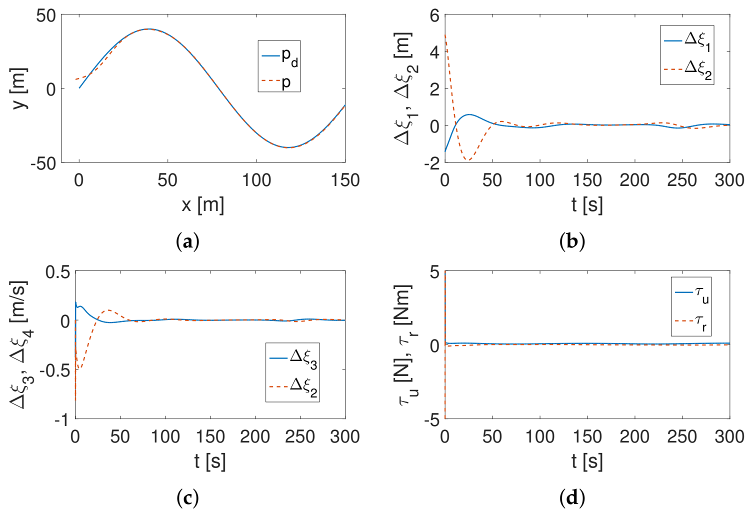

Figure 5. Simulation results for ROPOS original controller (CL) and sine trajectory: (**a**) desired and realized trajectory; (**b**) position error states; (**c**) velocity error states; and (**d**) applied force and torque.

4.2. XX AUV Model Vehicle

In order to test performance of the control algorithms the model of XX AUV underwater vehicle, described in [68], was chosen. It is a torpedo-shape vehicle. Its parameters are collected in Table 2. The parameters set means, that $N_1 = 47.5$ kg, and $N_2 = 94.1$ kg, $N_3 = 13.3$ kg$\cdot$m^2. For the point h, value $l = 1.5$ m was assumed.

For this vehicle $\|\Upsilon^{-1}\| = 1.0280$, which means about 5% couplings (1 is equivalent to 0% whereas 1.0732 to 10%). This value means that the couplings are very weak.

The set of gains applied for the QV controller was (50) whereas for the CL one (51) both for tracking of the linear and the sine trajectory. However, due to the dynamics of the XX AUV for the QV algorithm, it was assumed that $s_f = 10^{-1}$, $s_f N_1 = 4.75$, and $s_f N_3 = 1.33$.

Linear trajectory. The results for linear trajectory tracking are presented in Figure 6 (QV controller).

From Figure 6a, it can be concluded about the correct work of the control algorithm because the desired trajectory is tracked. Figure 6b,c show that after about 40 s, the position and velocity error states are close to zero. The applied force and torque (Figure 6d) have great values only if the vehicle starts, next their values are small. It results from the assumed initial point. It is clear from Figure 6e that the largest part of kinetic energy is dissipated in lateral motion v_r and half less in longitudinal motion u_r. The error $\Delta\zeta_2$ shown in Figure 6f has small values, which means that the impact of dynamic parameters on lateral movement is also very small.

The kinetic energy average values are $K_m = 39.45$ J (and $K_{m1} = 11.80$, $K_{m2} = 27.63$, $K_{m3} = 0.02$).

Figure 7 shows results obtained using the original controller [56]. As it is observed from Figure 7a, the desired trajectory is tracked but the position and velocity error states (Figure 7b,c) go to zero slower than for the QV control algorithm, i.e., after about 90 s. The applied force and torque (Figure 7d) have comparable values as for the previous controller. Other information is not available.

Sine trajectory. For the QV control algorithm, the results are shown in Figure 8, whereas for CL algorithm in Figure 9.

It can be clearly seen from Figure 8a that the QV controller works correctly. This observation is confirmed in Figure 8a,b, where the position and velocity error states are presented (the steady state is achieved after about 50 s). Moreover, the deviations of these errors are small taking into account the realized trajectory. The applied force and torque have great values only in the first phase of the vehicle's motion (Figure 8d). The kinetic energy consumption is presented in Figure 8e. As can be seen, the dominant consumption of this energy is caused by transverse movement of the vehicle, i.e., v_r. Only in the first phase the forward motion (u_r) causes the highest energy consumption. From Figure 8f, it can be concluded about the weak influence of dynamic parameters on the change in lateral velocity of the vehicle.

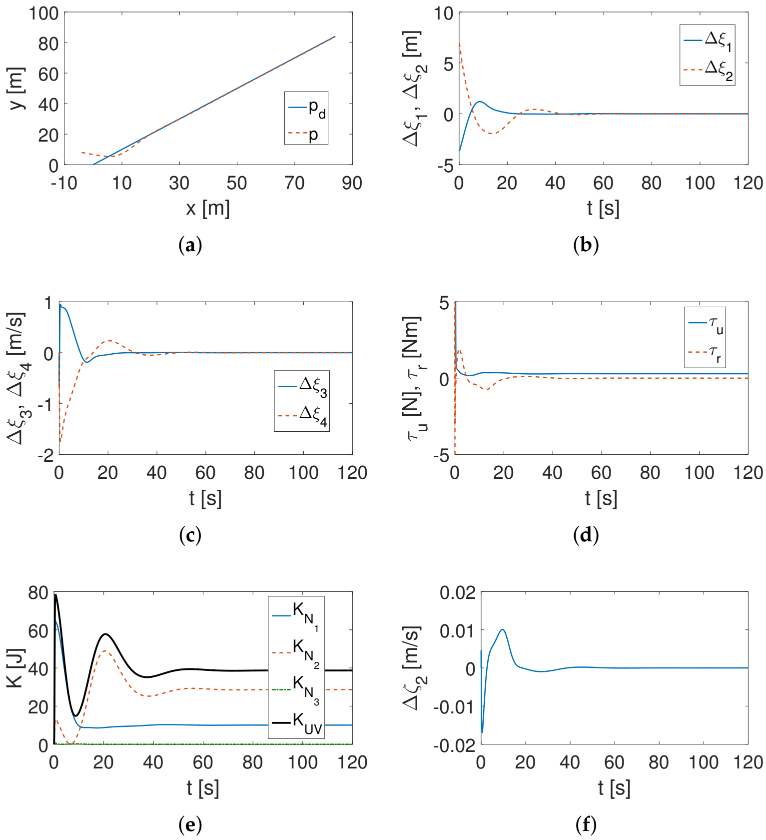

Figure 6. Simulation results for XX AUV QV controller and linear trajectory: (**a**) desired and realized trajectory; (**b**) position error states; (**c**) velocity error states; (**d**) applied force and torque; (**e**) kinetic energy time history; and (**f**) error $\Delta\zeta_2$.

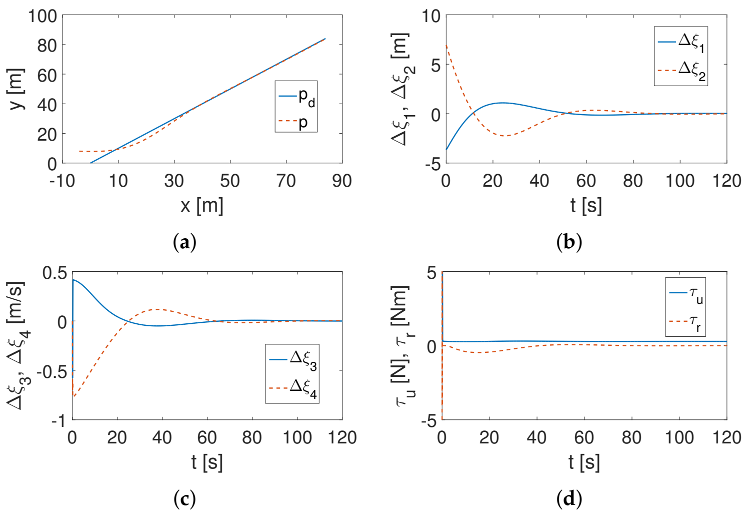

Figure 7. Simulation results for XX AUV original controller (CL) and linear trajectory: (**a**) desired and realized trajectory; (**b**) position error states; (**c**) velocity error states; and (**d**) applied force and torque.

The kinetic energy average values are $K_m = 19.04$ J (and $K_{m1} = 5.34$, $K_{m2} = 19.69$, $K_{m3} = 0.01$).

As can be seen in Figure 9a, the tracking task is carried out, but not quickly. However, taking into account Figure 9b,c, the position and velocity error states are not close to zero, but change as the vehicle moves, so trajectory tracking is inaccurate. Figure 9d shows that the values of applied force and torque are close to the values that were obtained using the QV control algorithm.

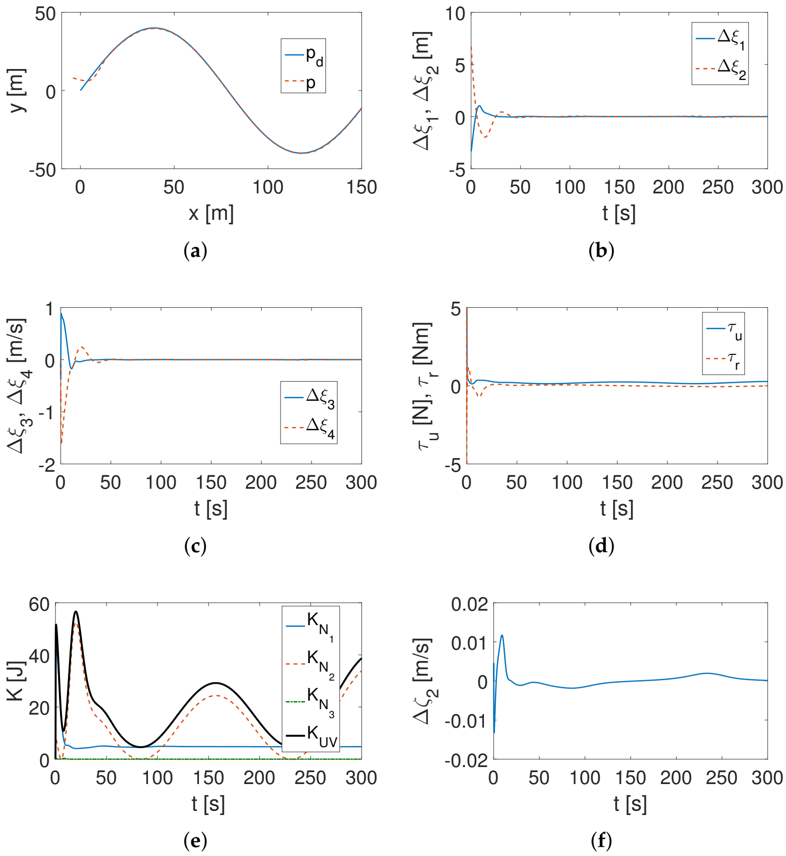

Figure 8. Simulation results for XX AUV QV controller and sine trajectory: (**a**) desired and realized trajectory; (**b**) position error states; (**c**) velocity error states; (**d**) applied force and torque; (**e**) kinetic energy time history; and (**f**) error $\Delta\zeta_2$.

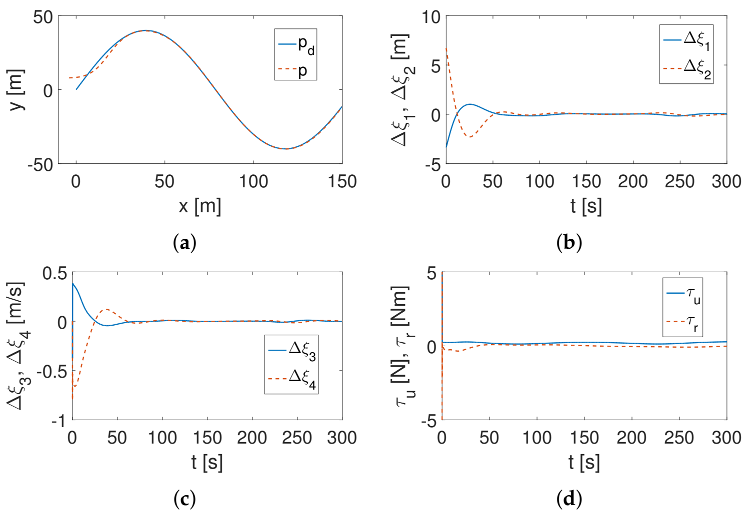

Figure 9. Simulation results for XX AUV original controller (CL) and sine trajectory: (**a**) desired and realized trajectory; (**b**) position error states; (**c**) velocity error states; and (**d**) applied force and torque.

4.3. Discussion of Results

Some observation based on the simulation results can be made.

(1) It turned out that for the control algorithm in the QV version, the same set of gains allows the tracking task to be carried out for both two different trajectories and two vehicles with significantly different dynamics. Such information proves a certain universality of a correctly selected set of controller gains.
(2) The coefficients that give satisfactory performance using the QV algorithms can be used to select the gains of a classic controller. For example the obtained gains set using QV $k_{v_x} = k_{v_y} = 4$, $k_{p_x} = k_{p_y} = 1$, $k_{I_x} = k_{I_y} = 0.25$, suggests that for ROPOS the gains for the CL algorithm may be chosen as follows: $k_{v_x} = k_{v_y} = 20 \div 30$, $k_{p_x} = k_{p_y} = 5 \div 10$, $k_{I_x} = k_{I_y} = 1 \div 2$. For example the obtained gains set using QV $k_{v_x} = k_{v_y} = 4$, $k_{p_x} = k_{p_y} = 1$, $k_{I_x} = k_{I_y} = 0.25$ for XX AUV model, suggests that the gains for the CL algorithm may be chosen as follows: $k_{v_x} = 10 \div 20$, $k_{v_y} = 5 \div 10$, $k_{p_x} = 3 \div 8$, $k_{p_y} = 1 \div 5$, $k_{I_x} = 1.0 \div 1.5$, $k_{I_y} = 0.2 \div 0.5$.
(3) Both algorithms (QV and CL) make it possible to track a desired trajectory with the use of small values of applied forces and torques, which is also consistent with the results shown in [56].
(4) It was found that significant changes in the vehicle dynamic parameters do not cause a significant deformation of the lateral velocity (the remaining quasi-speeds are equal to the velocities in the respective directions of movement).

5. Further Discussion on the Tracking Control Algorithm

5.1. The Proposed Controller versus Other Control Schemes

This section discusses the differences between the proposed control algorithm (PCA) and other selected schemes in recent years. The selected methods are classified into the following groups:

- Control strategies based on combinations of neural networks with other methods [31,35–38,49,50,52,69,70];
- Sliding mode control based approaches [18] or combined with backstepping [27];
- Control schemes with guaranteed prescribed performance [41,42,71,72];
- Extended observer based control algorithms [28,57–60];
- Fuzzy logic based control [40];
- Modified dynamic inversion [46];
- Input–output linearization [56].

In [31], the neural shunt model method was applied in order to solve the problem arising from virtual control law. The adaptive control strategy used a combination of backstepping sliding mode. Numerical simulation of trajectory tracking performed on a benchmark prototype and for circular trajectory showed the superiority of the algorithm compared to a known sliding control type method (with model uncertainty and environmental disturbances).

In [35], an adaptive trajectory tracking control strategy for an underactuated surface vehicle subject to unknown dynamics and time-varying external disturbances was presented. It consisted of first-order sliding mode, second-order sliding mode and the neural network minimum learning parameter method. The latter method was introduced into the design of controller. Numerical simulations were performed for straight and circular trajectories and the results obtained showed the effectiveness of tracking and were slightly better than for the sliding mode tracking control method selected from the literature (chattering was avoided).

Paper [36] addressed the control problem of trajectory tracking by underactuated autonomous surface vehicles with parameter uncertainty and nonlinear external disturbances. The control strategy included backstepping method, neural network and sliding mode control. The radial basis function neural network (RBFNN) was applied for estimation and approximation of unknown functions representing uncertainties due to its simplicity and linear parameterization. Simulation studies were carried out on a ship model taken from the literature and a desired sinusoidal trajectory and with sinusoidal external disturbances. The proposed neural-based command filtered backstepping (NBCFB) approach was compared with the traditional backstepping method and dynamic surface control (DSC) tracking based on neural network observer. Lower trajectory tracking errors were achieved and oscillations of position and velocity error signals were reduced.

In paper [37], a control algorithm for underactuated autonomous underwater vehicle is proposed which is a combination of Radial Basis Function (RBF) neural network algorithm and state prediction using sliding mode control method and backstepping. A sinusoidal trajectory was used for the simulation. The study found that the vehicle under the controller could track the desired trajectory at the highest speed to achieve accurate tracking of the desired trajectory. However, the velocity and input signal errors contained oscillations, which was a significant shortcoming of the algorithm. In addition, there was no simulation comparison study with another controller.

The problem of marine surface vessels (MSVs) tracking control in the presence of uncertain dynamics and external disturbances was investigated in [38]. The facts that actuators are subject to undesirable faults and input saturation are taken into consideration. Moreover, the event-triggered control (ETC) technique was applied. The proposed ETC was compared using simulations with the continuous control scheme for a ship model called CyberShip II as an example. The results were for only one trajectory and the tracking errors were not significantly different in both cases.

Chen et al. [49] proposed an adaptive trajectory tracking control algorithm for unmanned surface vehicles (USVs) with guaranteed transient performance. To make the dynamic USV model more realistic, it was assumed that the mass and damping matrices were not diagonal and the problem of input data saturation was taken into account. Neural networks (NN) were used to approximate the unknown external disturbances and uncertain hydrodynamics of the considered vehicles. The performance of the controller was verified by simulation and experimental studies and compared to the performance of the PI controller.

In paper [50], the trajectory tracking problem for underactuated marine vehicles with predefined tracking error constraints was considered. The boundary functions of the predefined constraints were asymmetric and time-varying and allowed for quantitative evaluation of prescribed tracking error performance at both transient and steady-state stages. A novel approach to the control of the transverse function was also developed to introduce an additional control input in backstepping procedure. Due to unmodeled dynamic uncertainties and external disturbances, neural network (NN) approximators were used to estimate uncertain dynamics and disturbance observers. Then, an adaptive control based on NN approximators and disturbance estimators were developed to guarantee the efficiency of error tracking during the transient stage of online NN weight adaptations and disturbance estimates. The simulation results on one vehicle model were compared with model-based control results and showed the effectiveness of the proposed tracking controller.

In [52], a practical adaptive sliding mode control scheme for an underactuated unmanned surface vehicle using a neural network, an auxiliary dynamic system, sliding mode control, and backstepping in the presence of modeling uncertainty and input saturation was proposed. A radial basis function neural network with minimum learning parameter method was used for on-line approximation of the uncertain system dynamics. Numerical simulations performed for the CyberShip II model demonstrated the effectiveness of the control strategy. In comparison with sliding mode robust tracking control (known from literature), a reduction of position and velocity tracking errors was obtained (only for circular trajectory).

Pan et al. [69] developed a novel event-triggered, complex, real-time learning control strategy for trajectory tracking of underactuated marine surface vehicles considering unknown dynamics and unknown time-varying disturbances. Neural networks (NN) were used to approximate the unknown dynamics. Simulation studies were performed for a vehicle model adopted from the literature. The desired trajectory was circular and two cases with different disturbances were investigated. The controller was effective but its performance was not compared with some other algorithm.

Paper [70] addressed the problem of robust finite-time trajectory tracking control for underactuated unmanned surface vehicles (USVs) subject to model uncertainty, saturation constraints, and external disturbances. An output redefinition-based dynamic transformation (ORDT) was utilized and next a sliding mode controller (SMC) was proposed that had the properties of chattering-free and finite time convergence. RBFNN-type neural networks were used to obtain an accurate identification of any continuous function describing unknown parameters of the model and external disturbances. Numerical simulations were performed to demonstrate the validity and effectiveness of the proposed approach. Three different external disturbances were tested on one type of surface vehicle.

In [18], the problem of robust tracking of a desired trajectory for underactuated marine vehicles was solved using a finite-time sliding mode control method. The controller design was divided into two stages: the design of the desired velocity and finite-time controller design. A new sliding mode surface was proposed that allowed stabilization of position tracking errors in finite time. The results of simulation studies that showed the effectiveness of the control scheme were only for one vehicle model (with a mass of about 2 kg) and were not compared with the results of another algorithm.

Sun et al. [27] proposed a sliding mode controller to solve the problem of trajectory tracking of an underactuated surface vessel. By combining adaptive continuous sliding mode control with a backstepping method, the chattering phenomenon reducing and the trajectory tracking problem were successfully solved. Moreover, a novel sliding mode PI control was designed, which made the control scheme more practical. In the simulation studies, one marine vehicle model was tested and for one complex desired trajectory. The control algorithm was found to be effective in the trajectory tracking task, but its effectiveness was not compared in the simulations with that of another controller.

The control problem of tracking the trajectory of underactuated surface vessels using a quantitative method with only position and attitude available was considered in [41]. Using a combination of a high-gain observer, a parameter compression algorithm, and a performance function, an adaptive control strategy with a given performance was presented. A high-gain observer was constructed for velocity estimation, and the parameter compression algorithm was used to account for persistent perturbations and model uncertainties in a more concise manner. The controller guaranteed the prescribed performance. Numerical simulations were performed for one ship model (taken from the literature) and one desired trajectory. The control scheme proved to be effective and slightly smaller trajectory tracking errors were obtained compared to another tested algorithm.

Li et al. [42] developed a novel robust adaptive control scheme for trajectory tracking with prescribed performance for autonomous underwater vehicles in horizontal motion subject to unknown dynamic parameters and disturbances. A simple error mapping function was proposed to ensure that the trajectory tracking error meets the prescribed performance. In addition, a novel control based on the Nussbaum function was added to deal with the underactuation of the marine vehicle. The simulations presented were for one vehicle, tracking a desired sinusoidal trajectory for two different disturbances functions. In both cases, the controller worked correctly and was effective.

In [71], a new adaptive performance control (PPC) strategy was presented for a class of USVs when parametric uncertainty and external disturbances were present. Prescribed performance and steady-state performance in terms of trajectory tracking velocity and accuracy were achieved using continuous and singularity-free control. In addition, the controller eliminated the need for disturbance observers and the assumption that disturbances must be differentiable. A simulation study performed on one ship model confirmed the effectiveness of the controller. It also turned out that the offered approach outperforms in terms of tracking performance (less error perturbation) the method selected from the literature for comparison.

Park and Yoo [72] proposed a robust control methodology based on to track the trajectories of uncertain USVs under the presence of external disturbances in a band-limited network environment. They used a coordinate transformation method and an auxiliary signal to solve the problem of insufficient activation of a USV model (with asymmetric stern and bow). They assumed that all USV states and inputs are quantized by a uniform quantizer, which was designed using a low-complexity PPC method. The proposed quantized feedback tracking system consisted of performance functions and error surfaces using quantized states, which did not require any adaptive techniques. Conditions for the selection of the performance functions were also given. Simulation results shown that the proposed control strategy was effective for the control problem under a band-limited network with state and input quantization. Comparison of the proposed method with another taken from the literature (for one vehicle) showed slightly smaller tracking error results for the assumed complex trajectory.

In [28], the problem of horizontal trajectory tracking control for underactuated marine vehicles subject to unknown internal and external disturbances was considered. The control design involved two stages. First, a kinematic control law of the desired surge speed and trajectory angle was derived. Then, a kinematic control law that satisfies the convergence requirement was designed. Specifically, the kinetic law was divided into two components: the control law of disturbance rejection control law and the stabilization control law. The former was obtained from the high gain ESO, which was designed to estimate unknown disturbances, and the latter was developed in a reduced model using backstepping method and composite-system method. The main advantage of the proposed approach is that the design and analysis process has been simplified to some extent. Simulation verification was performed for a model known from the literature and three trajectories: circular, sinusoidal and complex. Based on the results obtained, the authors concluded that the validity and effectiveness of the proposed method and the proposed control scheme have been sufficiently proven.

Xia et al. [57] demonstrated the design of an improved line-of-sight (LOS) based adaptive trajectory tracking controller for an underactuated marine vehicle subject to highly coupled nonlinearities, ocean currents-induced uncertainties, and input saturation. The strategy was composed of LOS, terminal sliding mode control (TSMC), and extended disturbance observers (EDO). The LOS guidance law was used to steer the vehicle towards the desired trajectory. The TSMC improved system robustness and asymptotic convergence, and was applied to weaken the influence of actuator saturation. The extended disturbance observers estimated the ocean current-induced disturbances in the kinematic model. Effectiveness and robustness of the proposed trajectory tracking was verified by numerical simulations on a well-known AUV REMUS vehicle. Four cases were considered for this control scheme, which confirmed the theoretical results.

Paper [58] was devoted to solving a full-state control (FSRC) problem for an asymmetric underactuated surface vehicle (AUSV) subject to disturbances. The FSRC objective was divided into two subtasks, i.e., reaching trajectory (RT) guidance and synthesis of a tracking controller with underactuation and disturbances. After performing a series of coordinate transformations, the tracking error dynamics were shaped as a translational–rotational cascade with respect to the central frame of the circular orbit. Utilizing a finite-time method, the lumped disturbances were accurately estimated by accurate observers, facilitating the synthesis of the surge and yaw controllers. The effectiveness of the proposed approach was demonstrated using simulations on the CyberShip II prototype. However, no comparison with the results of another controller was shown.

In [59], the problem of accurately controlling the trajectory tracking of an asymmetric underactuated surface vehicle (AUSV) was solved by guiding yaw dynamics, which were free of persistent excitation (PE). Next, a nested coordinate transformations was applied in order to formulate the AUSV model in a cascade structure consisting of translation and rotation subsystems with complex uncertainties. Finite time uncertainty observers (FUOs) were developed to accurately estimate the transformed uncertainties and enable the application of the separation principle in controller and observer syntheses. The global asymptotic stability of the whole translation–rotation tracking system was obtained and a FUO-based yaw-guided tracking control (FUO-YTC) scheme was developed for an AUSV with complex uncertainties. In simulation studies on the CyberShip II prototype, the authors focused on comparing the performance of different versions of the proposed control scheme for tracking three desired trajectories namely straight line, circle, and curve. The tracking accuracy strongly depended on the variant of the controller used.

In paper [60], a decoupling and yaw control strategy was proposed for a USV to maintain a constant speed and a desired course for high performance of on-board sonar during seabed exploration. In addition to the direct Lyapunov method, a hierarchical stepwise control method was used to achieve the desired speed and yaw angle of the vehicle under the influence of external disturbances such as wind, waves, and currents. An disturbance observer was also constructed to compensate for oscillations occurring with external disturbances. The validity and robustness of the decoupling controller was verified by application to one model of USV and straight line tracking.

Wang et al. [40] proposed an adaptive online constructive fuzzy controller (AOCFC) for tracking USV trajectories while ensuring system stability. A new online constructive fuzzy approximator (OCFA) was integrated with the dynamic surface control (DSC) method to estimate the unknown time-variable uncertainty. Compared with the fixed-structure fuzzy regulator, the proposed online constructive fuzzy regulator strategy was able to adapt the online fuzzy rules to ensure the sufficiency and simplicity of the fuzzy system. In the simulation study (on one vehicle model), the fuzzy control algorithm (AOCFC) was compared with the adaptive structure-fixed fuzzy control (ASFFC) to show the effectiveness and advantages of the constructive online fuzzy strategy.

Ye and Zong [46] presented three modified dynamic inversion methods for tracking control of underactuated ship. In the first called dynamic extension-based on dynamic expansion (DEDI) the input was treated as a state and dynamic expansion was used to obtain the relative degree. The second method, i.e., virtual input-based dynamic inversion (VIDI), treating the state as a virtual input to obtain the relative degree. The third method was output redefinition-based dynamic inversion (ORDI), selecting a specific variable as a new output to achieve relative degree. These three methods were generalizations of dynamic inversion control and eliminate some of its limitations, so they could be applied to a wide variety of underactuated systems. Numerical simulations performed on one selected vehicle demonstrated the effectiveness of the control approach. Furthermore, a comparison with a reference method was presented.

In [56], a trajectory tracking strategy and and path control strategy for underactuated marine vehicles were presented. The strategy was developed as an extension of the results of the work on ground vehicles, which introduced the hand position point definition to marine vehicles (the definition of the hand position point was extended). An input–output feedback linearization method using hand position as output was applied and a trajectory tracking strategy and a path following strategy were developed for general paths, with straight line paths as a special case. The effects of environmental disturbances, such as a steady and non-rotating ocean current, on the vehicle were also considered. The effectiveness of the approach was confirmed using simulation studies on the model and experimental studies on the real vehicle.

It is worthwhile to present the differences between the selected methods and the control scheme using quasi-velocities. The method proposed in this paper is intended not only to realize the trajectory tracking of the desired control but also to provide some insight into the dynamics of the vehicle in motion also under the influence of external disturbances. For this reason, only some of the control strategies would be suitable to realize the objective of the work.

Methods based on the use of neural networks require additional mathematical knowledge. Similarly, any complicated control algorithm makes difficult the dynamics analysis proposed in this work. The reason for this is that to show the changes in vehicle dynamics while tracking the desired trajectory, a velocity transformation that diagonalizes the inertia matrix is sufficient. However, without the velocity transformation, no insight into the dynamics of the system will be obtained so as to estimate the impact of mechanical couplings in for the assumed model and trajectory type.

Methods containing observers are also not useful for analyzing dynamics for coupling estimation because the additional system (observer) introduces its own dynamics into the original model. Control algorithms with prescribed performance are supposed to lead to signals within prescribed limits. In contrast, the presented scheme is concerned not only with achieving the control objective, but also with studying the impact of coupling during performing the primary task.

Comparative simulations were performed only with the input-output feedback linearization method developed in [56] to show the differences resulting from the application of the classical asymmetric vehicle model and the model obtained by means of the velocity transformation. In the original method, the accelerations are coupled in such a way that the inertial forces cannot be attributed to only one variable. On the contrary, when the dynamics is described in quasi-velocities the mechanical couplings occurring in the system as their effect on the vehicle motion can be estimated. The original control algorithm is used for tracking while the one presented in this paper, in addition to accomplishing the control task, also provides insight into vehicle dynamics.

Since the symmetric inertia matrix plays a key role for the proposed controller, from this point of view the control methods can be divided into:

- Methods for the model with a diagonal inertia matrix [18,27,28,31,35–38,40–42,46,71];
- Methods for the model with a symmetric inertia matrix [49,50,52,56–60,72].

Control methods designed for the dynamics model with diagonal inertia matrix cannot be compared with the proposed algorithm because it is suitable for estimating the effect of dynamic couplings. If a diagonal inertia matrix is adopted in the model, it is assumed that any inaccuracies due to inertial forces will be compensate by the control algorithm. The proposed scheme can also be applied to a model with a diagonal matrix, but then it will only be used for control purposes and not to estimate the effect of couplings on the vehicle behavior.

5.2. Advantages and Benefits of the Control Approach

The advantages and benefits of the proposed velocity transformation based control scheme can be summarized as follows:

- It is suitable for the control of asymmetric vehicles, which makes the dynamics model more realistic than the model with a diagonal inertia matrix;
- In comparison with other algorithms, after the velocity transformation from the modified controller, additional information hidden in the inertia matrix can be obtained;
- It gives ability to estimate the effect of couplings on vehicle behavior in motion (this effect can be studied for various trajectories and vehicles, e.g., to change them);
- It can be used for both diagonal and non-diagonal inertia matrix models to decide whether the simplified model is sufficient.

6. Conclusions

In this work, the tracking problems of the trajectory tracking for underactuated underwater marine vehicles is addressed. An application of the trajectory tracking algorithm expressed in terms of quasi-velocities was proposed and tested in simulations. The QV-based first-order equations of motion arise from the velocity transformation and allows to decouple the accelerations. The modified control algorithm uses those QV and it is slightly different than the original algorithm proposed in [56]. By analyzing the simulation results with the use of both trajectory tracking algorithms (QV and CL), it can be concluded that they are suitable for various underwater vehicles and different types of these trajectories provided that the velocity disturbance is small (less than 0.1 m/s). Information on vehicle dynamics that can be obtained using the quasi-velocities has been pointed out. It has also been shown that some information about the dynamics of the vehicle is not available if we apply the classical equations of motion. There was also a discussion on the offered controller and control schemes selected from the literature published in recent years. The advantages of its application were also mentioned. Summarizing the modified equations and the control algorithm are useful not only to control the underwater vehicle, but also to gain insight into its dynamics.

Funding: The work was supported by Poznan University of Technology Grant No. 0211/SBAD/0121.

Institutional Review Board Statement: Not applicable.

Informed Consent Statement: Not applicable.

Data Availability Statement: Not applicable.

Conflicts of Interest: The author declares no conflict of interest.

References

1. Song, F.; An, E.; Folleco, A. Modeling and Simulation of Autonomous Underwater Vehicles: Design and Implementation. *IEEE J. Ocean. Eng.* **2003**, *28*, 283–296. [CrossRef]
2. American Bureau of Shipping. *ABS Guide for Vessel Maneuverability*; American Bureau of Shipping: Houston, TX, USA, 2006; Updated February 2017.
3. Do, K.D.; Pan, J. *Control of Ships and Underwater Vehicles*; Springer: London, UK, 2009.
4. Wang, C.; Zhang, F.; Schaefer, D. Dynamic modeling of an autonomous underwater vehicle. *J. Mar. Sci. Technol.* **2015**, *20*, 199–212. [CrossRef]
5. Min, F.; Pan, G.; Xu, X. Modeling of Autonomous Underwater Vehicles with Multi-Propellers Based on Maximum Likelihood Method. *J. Mar. Sci. Eng.* **2020**, *8*, 407. [CrossRef]
6. Miao, J.; Wang, S.; Tomovic, M.M.; Zhao, Z. Compound line-of-sight nonlinear path following control of underactuated marine vehicles exposed to wind, waves, and ocean currents. *Nonlinear Dyn.* **2017**, *89*, 2441–2459. [CrossRef]
7. Battista, T.; Woolsey, C. Control of an Underwater Vehicle in Irregular Waves. In Proceedings of the OCEANS 2015—MTS/IEEE Washington, Washingtton, DC, USA, 19–22 October 2015.
8. Zhang, G.; Zhang, C.; Zhang, X.; Deng, Y. ESO-based path following control for underactuated vehicles with the safety prediction obstacle avoidance mechanism *Ocean. Eng.* **2019**, *174*, 14–30.
9. Wiig, M.S.; Pettersen K.Y.; Krogstad T.R. Collision Avoidance for Underactuated Marine Vehicles Using the Constant Avoidance Angle Algorithm. *IEEE Trans. Control. Syst. Technol.* **2020**, *28*, 951–966. [CrossRef]
10. Liu J.; Zhao, B.; Li, L. Collision Avoidance for Underactuated Ocean-Going Vessels Considering COLREGs Constraints. *IEEE Access* **2021**, *9*, 145943–145954. [CrossRef]
11. Woods, S.A.; Bauer, R.J.; Seto, M.L. Automated Ballast Tank Control System for Autonomous Underwater Vehicles. *IEEE J. Ocean. Eng.* **2012**, *37*, 727–739. [CrossRef]
12. Rosario, R.V.C.; Cunha, J.P.V.S.; Garcia-Rosa, P.B. Stabilizing Control of an Unmanned Surface Vehicle Pushing a Floating Load. *Int. J. Control. Autom. Syst.* **2020**, *18*, 3194–3203. [CrossRef]
13. Behal, A.; Dawson, D.M.; Dixon, W.E.; Fang, Y. Tracking and Regulation Control of an Underactuated Surface Vessel With Nonintegrable Dynamics. *IEEE Trans. Autom. Control.* **2002**, *47*, 495–500. [CrossRef]
14. Jiang, Z.P. Global tracking control of underactuated ships by Lyapunov's direct method. *Automatica* **2002**, *38*, 301–309. [CrossRef]
15. Lefeber, E.; Pettersen, K.Y.; Nijmeijer, H. Tracking Control of an Underactuated Ship. *IEEE Trans. Control. Syst. Technol.* **2003**, *11*, 52–61. [CrossRef]
16. Ashrafiuon, H.; Muske, K.R.; McNinch, L.C.; Soltan, R.A. Sliding-Mode Tracking Control of Surface Vessels. *IEEE Trans. Ind. Electron.* **2008**, *55*, 4004–4012. [CrossRef]
17. Elmokadem, T.; Zribi, M.; Youcef-Toumi K. Trajectory tracking sliding mode control of underactuated AUVs. *Nonlinear Dyn.* **2016**, *84*, 1079–1091. [CrossRef]
18. Zhang, L.; Huang, B.; Liao, Y.; Wang, B. Finite-Time Trajectory Tracking Control for Uncertain Underactuated Marine Surface Vessels. *IEEE Access* **2019**, *7*, 102321–102330 [CrossRef]
19. Elmokadem, T.; Zribi, M.; Youcef-Toumi, K. Terminal sliding mode control for the trajectory tracking of underactuated Autonomous Underwater Vehicles. *Ocean. Eng.* **2017**, *129*, 613–625. [CrossRef]
20. Qiao, L.; Zhang, W. Fast Trajectory Tracking Control of Underactuated Autonomous Underwater Vehicles. In Proceedings of the 8th IEEE International Conference on Underwater System Technology: Theory and Application, USYS 2018, Wuhan, China, 1–3 December 2018; pp. 1–6.

21. Yan, Z.; Yu, H.; Zhang, W.; Li, B.; Zhou, J. Globally finite-time stable tracking control of underactuated UUVs. *Ocean Eng.* **2015**, *107*, 132–146. [CrossRef]
22. Godhavn J.M.; Fossen, T.I.; Berge, S.P. Non-Linear and Adaptive Backstepping Designs for Tracking Control of Ships. *Int. J. Adapt. Control. Signal Process.* **1998**, *12*, 649–670. [CrossRef]
23. Repoulias, F.; Papadopoulos, E. Planar trajectory planning and tracking control design for underactuated AUVs. *Ocean Eng.* **2007**, *34*, 1650–1667. [CrossRef]
24. Xie, W.J.; Ma, B.L. Universal Practical Tracking Control of Planar Underactuated Vehicle. *Asian J. Control.* **2015**, *17*, 1016–1026.
25. Do, K.D. Robust adaptive tracking control of underactuated ODINs under stochastic sea loads. *Robot. Auton. Syst.* **2015**, *72*, 152–163. [CrossRef]
26. Do, K.D. Global Inverse Optimal Tracking Control of Underactuated Omni-directional Intelligent Navigators (ODINs). *J. Mar. Sci. Appl.* **2015**, *14*, 1–13. [CrossRef]
27. Sun, Z.; Zhang, G.; Qiao, L.; Zhang, W. Robust adaptive trajectory tracking control of underactuated surface vessel in fields of marine practice. *J. Mar. Sci. Technol.* **2018**, *23*, 950–957. [CrossRef]
28. Lei, M.; Li, Y.; Pang, S. Extended state observer-based composite-system control for trajectory tracking of underactuated AUVs. *Appl. Ocean. Res.* **2021**, *112*, 102694. [CrossRef]
29. Pettersen, K.Y.; Nijmeijer, H. Global practical stabilization and tracking for an underactuated ship—A combined averaging and backstepping approach. *Model. Identif. Control.* **1999**, *20*, 189–199. [CrossRef]
30. Sun, B.; Zhu, D.; Ding, F.; Yang, S.X. A novel tracking control approach for unmanned underwater vehicles based on bio-inspired neurodynamics. *J. Mar. Sci. Technol.* **2013**, *18*, 63–74. [CrossRef]
31. Zhao, Y.; Sun, X.; Wang, G.; Fan, Y. Adaptive Backstepping Sliding Mode Tracking Control for Underactuated Unmanned Surface Vehicle With Disturbances and Input Saturation. *IEEE Access* **2021**, *9*, 1304–1312. [CrossRef]
32. Do, K.D.; Jiang, Z.P.; Pan, J.; Nijmeijer H. A global output-feedback controller for stabilization and tracking of underactuated ODIN: A spherical underwater vehicle. *Automatica* **2004**, *40*, 117–124. [CrossRef]
33. Pan, C.Z.; Lai, X.Z.; Wang, S.X.; Wu, M. An efficient neural network approach to tracking control of an autonomous surface vehicle with unknown dynamics. *Expert Syst. Appl.* **2013**, *40*, 1629–1635. [CrossRef]
34. Zhang, L.J.; Qi, X.; Pang, Y.J. Adaptive output feedback control based on DRFNN for AUV. *Ocean Eng.* **2009**, *36*, 716–722. [CrossRef]
35. Mu, D.; Wang, G.; Fan, Y.; Qiu, B.; Sun, X. Adaptive Trajectory Tracking Control for Underactuated Unmanned Surface Vehicle Subject to Unknown Dynamics and Time-Varing Disturbances. *Appl. Sci.* **2018**, *8*, 547. [CrossRef]
36. Zhang, C.; Wang, C.; Wei, Y.; Wang, J. Neural-Based Command Filtered Backstepping Control for Trajectory Tracking of Underactuated Autonomous Surface Vehicles. *IEEE Access* **2020**, *8*, 42482–42490. [CrossRef]
37. Zhou, J.; Zhao, X.; Chen, T.; Yan, Z.; Yang, Z. Trajectory Tracking Control of an Underactuated AUV Based on Backstepping Sliding Mode With State Prediction. *IEEE Access* **2019**, *7*, 181983–181993. [CrossRef]
38. Zhu, G.; Ma, Y.; Li, Z.; Malekian, R.; Sotelo, M. Event-Triggered Adaptive Neural Fault-Tolerant Control of Underactuated MSVs With Input Saturation. *IEEE Trans. Intell. Transp. Syst.* **2021**, 1–13. [CrossRef]
39. Raimondi, F.M.; Melluso, M. Fuzzy/kalman hierarchical horizontal motion control of underactuated ROVs. *Int. J. Adv. Robot. Syst.* **2010**, *7*, 139–154. [CrossRef]
40. Wang, S.; Fu, M.; Wang, Y.; Tuo, Y.; Ren, H. Adaptive Online Constructive Fuzzy Tracking Control for Unmanned Surface Vessel With Unknown Time-Varying Uncertainties. *IEEE Access* **2018**, *6*, 70444–70455. [CrossRef]
41. Jia, Z.; Hu, Z.; Zhang, W. Adaptive output-feedback control with prescribed performance for trajectory tracking of underactuated surface vessels. *ISA Trans.* **2019**, *95*, 18–26. [CrossRef]
42. Li, J.; Du, J.; Sun, Y.; Lewis, F.L. Robust adaptive trajectory tracking control of underactuated autonomous underwater vehicles with prescribed performance. *Int. J. Robust Nonlinear Control.* **2019**, *29*, 4629–4643. [CrossRef]
43. Guerreiro, B.J.; Silvestre, C.; Cunha, R.; Pascoal, A. Trajectory Tracking Nonlinear Model Predictive Control for Autonomous Surface Craft. *IEEE Trans. Control. Syst. Technol.* **2014**, *22*, 2160–2175. [CrossRef]
44. Chwa, D. Global Tracking Control of Underactuated Ships With Input and Velocity Constraints Using Dynamic Surface Control Method. *IEEE Trans. Control Syst. Technol.* **2011**, *19*, 1357–1370. [CrossRef]
45. Harmouche, M.; Laghrouche, S.; Chitour, Y. Global tracking for underactuated ships with bounded feedback controllers. *Int. J. Control.* **2014**, *87*, 2035–2043. [CrossRef]
46. Ye, L.; Zong, Q. Tracking control of an underactuated ship by modified dynamic inversion. *ISA Trans.* **2018**, *83*, 100–106. [CrossRef] [PubMed]
47. Serrano, M.E.; Scaglia, G.J.E.; Godoy, S.A.; Mut, V.; Ortiz, O.A. Trajectory Tracking of Underactuated Surface Vessels: A Linear Algebra Approach. *IEEE Trans. Control Syst. Technol.* **2014**, *22*, 1103–1111. [CrossRef]
48. Panagou, D.; Kyriakopoulos, K.J. Viability control for a class of underactuated systems. *Automatica* **2013**, *49*, 17–29. [CrossRef]
49. Chen, L.; Cui, R.; Yang, C.; Yan, W. Adaptive Neural Network Control of Underactuated Surface Vessels with Guaranteed Transient Performance: Theory and Experimental Results. *IEEE Trans. Ind. Electron.* **2020**, *67*, 4024–4035. [CrossRef]
50. Dai, S.L.; He, S.; Lin, H. Transverse function control with prescribed performance guarantees for underactuated marine surface vehicles. *Int. J. Robust Nonlinear Control.* **2019**, *29*, 1577–1596. [CrossRef]

51. Park, B.S. Neural Network-Based Tracking Control of Underactuated Autonomous Underwater Vehicles With Model Uncertainties. *J. Dyn. Syst. Meas. Control. Trans. ASME* **2015**, *137*, 021004. [CrossRef]
52. Qiu, B.; Wang, G.; Fan, Y.; Mu, D.; Sun, X. Adaptive Sliding Mode Trajectory Tracking Control for Unmanned Surface Vehicle with Modeling Uncertainties and Input Saturation. *Appl. Sci.* **2019**, *9*, 1240. [CrossRef]
53. Dong, Z.; Wan, L.; Liu, T.; Zeng, J. Horizontal-plane Trajectory-tracking Control of an Underactuated Unmanned Marine Vehicle in the Presence of Ocean Currents. *Int. J. Adv. Robot. Syst.* **2016**. [CrossRef]
54. Zhang, Z.; Wu, Y. Further results on global stabilisation and tracking control for underactuated surface vessels with non-diagonal inertia and damping matrices. *Int. J. Control.* **2015**, *88*, 1679–1692. [CrossRef]
55. Ashrafiuon, H.; Nersesov, S.; Clayton, G. Trajectory Tracking Control of Planar Underactuated Vehicles. *IEEE Trans. Autom. Control.* **2017**, *62*, 1959–1965. [CrossRef]
56. Paliotta, C.; Lefeber, E.; Pettersen, K.Y.; Pinto, J.; Costa, M.; de Figueiredo Borges de Sousa J.T. Trajectory Tracking and Path Following for Underactuated Marine Vehicles. *IEEE Trans. Control Syst. Technol.* **2019**, *27*, 1423–1437. [CrossRef]
57. Xia, Y.; Xu, K.; Li, Y.; Xu, G.; Xiang, X. Improved line-of-sight trajectory tracking control of under-actuated AUV subjects to ocean currents and input saturation. *Ocean Eng.* **2019**, *174*, 14–30. [CrossRef]
58. Wang, N.; Xie, G.; Pan, X.; Su, S.F. Full-State Regulation Control of Asymmetric Underactuated Surface Vehicles. *IEEE Trans. Ind. Electron.* **2019**, *66*, 8741–8750. [CrossRef]
59. Wang, N.; Su, S.F.; Pan, X.; Yu, X.; Xie, G. Yaw-Guided Trajectory Tracking Control of an Asymmetric Underactuated Surface Vehicle. *IEEE Trans. Ind. Inform.* **2019**, *15*, 3502–3513. [CrossRef]
60. Wang, C.; Xie, S.; Chen, H.; Peng, Y.; Zhang, D. A decoupling controller by hierarchical backstepping method for straight-line tracking of unmanned surface vehicle. *Syst. Sci. Control. Eng.* **2019**, *7*, 379–388. [CrossRef]
61. Loduha, T.A.; Ravani, B. On First-Order Decoupling of Equations of Motion for Constrained Dynamical Systems. *Trans. ASME J. Appl. Mech.* **1995**, *62*, 216–222. [CrossRef]
62. Herman, P. Velocity tracking controller for simulation analysis of underwater vehicle model. *J. Mar. Eng. Technol.* **2020**, *19*, 229–239. [CrossRef]
63. Herman, P. Application of nonlinear controller for dynamics evaluation of underwater vehicles. *Ocean Eng.* **2019**, *179*, 59–66. [CrossRef]
64. Herman, P. Numerical Test of Several Controllers for Underactuated Underwater Vehicles. *Appl. Sci.* **2020**, *10*, 8292. [CrossRef]
65. Fossen, T.I. *Guidance and Control of Ocean Vehicles*; John Wiley and Sons: Chichester, UK, 1994.
66. Lesniak, J.; Stachowiak, M. Simulation Analysis of Selected Vehicle Control Methods with Incomplete Input Signals. Engineering Thesis, Poznan University of Technology, Poznań, Poland, 2020.
67. Soylu, S.; Buckham, B.J.; Podhorodeski, R.P. A chattering-free sliding-mode controller for underwater vehicles with fault-tolerant infinity-norm thrust allocation. *Ocean Eng.* **2008**, *35*, 1647–1659. [CrossRef]
68. Dong, Z.; Wan, L.; Li, Y.; Liu, T.; Zhuang, J.; Zhang, G. Point Stabilization for an Underactuated AUV in the Presence of Ocean Currents. *Int. J. Adv. Robot. Syst.* **2015**, *12*, 1. [CrossRef]
69. Pan, B.; Chen, C.; Zhu, G.; Su, Y. Event-Triggered Composite Learning Finite-Time Trajectory Tracking Control for Underactuated MSVs Subject to Uncertainties. *IEEE Access* **2022**, *10*, 14440–14449. [CrossRef]
70. Zhang, L.; Zheng, Y.; Huang, B.; Su, Y. Finite-time trajectory tracking control for under-actuated unmanned surface vessels with saturation constraint. *Ocean Eng.* **2022**, *249*, 110745. [CrossRef]
71. Zhang, J.X.; Chai, T. Singularity-Free Continuous Adaptive Control of Uncertain Underactuated Surface Vessels With Prescribed Performance. *IEEE Trans. Syst. Man Cybern. Syst.* **2021**, 1–10. [CrossRef]
72. Park, B.S.; Yoo, J.Y. Robust trajectory tracking with adjustable performance of underactuated surface vessels via quantized state feedback. *Ocean Eng.* **2022**, *246*, 110475. [CrossRef]